CrystEngComm

ROYAL SOCIETY OF CHEMISTRY

COMMUNICATION

View Article Online
View Journal | View Issue

Cite this: *CrystEngComm*, 2021, **23**, 2513

Received 1st February 2021,
Accepted 19th March 2021

DOI: 10.1039/d1ce00159k

rsc.li/crystengcomm

The trimorphism of 3-hydroxybenzoic acid: an experimental and computational study†

Doris E. Braun

Following the computational prediction that 3-hydroxybenzoic acid (3HBA) could exist in more than the two literature polymorphs, an experimental investigation targeting computationally generated structures was performed. The third polymorph III, solved from powder X-ray diffraction data, and the literature form II share a common hydrogen-bonded ladder motif in contrast to the carboxylic acid dimer based form I. The two metastable polymorphs (II and III) are storage stable if phase pure and monotropically related to form I. Calorimetric measurements and (lattice) energy minimisations revealed that the three polymorphs are close in energy.

Depending on its chemical nature each compound may exist or can be designed in a number of solid-state forms (anhydrate, solvate/hydrate, cocrystal, amorphous form).[1,2] The increasing awareness that the solid form may have tremendous impact on materials properties (solubility, stability, *etc.*)[3–5] and consequently can profoundly influence industrial processes and the performance of a fine chemical (drug compound) triggered the research in the field of polymorphism. A hot class of solid-state forms are cocrystals, in particular since the 2018 US Food and Drug Administration (FDA) guidance on pharmaceutical cocrystals[6] has been released. Cocrystallisation involves the formation of novel materials containing at least two neutral molecules in a crystalline array.[7] Hydroxybenzoic acids are routinely investigated as coformers[8–10] because they have the potential to form strong hydrogen-bonding interactions to other functional groups. The acids are chemically simple, yet important molecules (*e.g.* ref. 11) and many have been found to exhibit polymorphism[12] and to form solvates.[13,14]

To extend previous studies on hydroxybenzoic acids (*e.g.* ref. 12, 13, 15 and 16), 3-hydroxybenzoic acid (3HBA, Fig. 1) was subjected to a complementary computational[17] and experimental investigation, with the aim to unravel polymorphism, preferential packing arrangements and the stability of the experimental forms. Single crystal structures of two polymorphs (form **I**,[18] monoclinic, CSD-refcode[19] BIDLOP; form **II**, orthorhombic, BIDLOP01 (ref. 18)/02 (ref. 20)) and their monotropic relationship, with form **I** being the stable form,[21] have already been reported.

The $Z' = 1$ & 2 crystal energy landscape (Fig. 2) was generated starting from the two low-energy conformers of the acid (Fig. 1),[22–24] allowing for conformational changes in the COOH function and the *m*-OH proton position[25–29] and estimating room temperature Helmholtz free energies in the rigid-body harmonic approximation,[30–32] as detailed in the ESI.†

The crystal energy landscape (Fig. 2) of 3HBA exhibits numerous structures, which are all in the energy range expected for polymorphism.[33,34] The two known polymorphs were found as the global minimum structure (form **I**) and the second most stable structure (form **II**), differing only by 0.58 kJ mol^{-1} in energy. The form **I** structure contains the common carboxylic acid $R_2^2(8)$ dimer motif[35] D (Fig. 3), whereas form **II** features a chain motif C, with alternate COOH and OH-groups creating a ribbon motif, C1 hereafter, composed of two C chain motifs. Overall, all of the 45 low-energy structures can be classified into the two groups

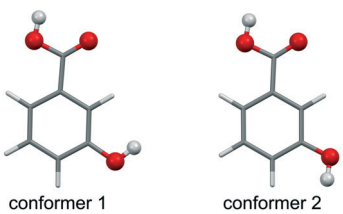

Fig. 1 Molecular diagram of 3-hydroxybenzoic acid low-energy conformers **1** and **2**, with conformer **1** being the global minimum and 3.25 kJ mol^{-1} more stable than conformer **2** (estimated at the PBE0/6-31G(d,p) level of theory).

Institute of Pharmacy, University of Innsbruck, Innrain 52c, 6020 Innsbruck, Austria. E-mail: doris.braun@uibk.ac.at

† Electronic supplementary information (ESI) available: Low-energy conformers, computational generation of the crystal energy landscape, packing comparisons, pairwise intermolecular energy calculations, powder X-ray diffraction, Rietveld refinement of form **III**, solution calorimetry, semi-schematic energy temperature diagram, and variable temperature IR spectroscopy. See DOI: 10.1039/d1ce00159k

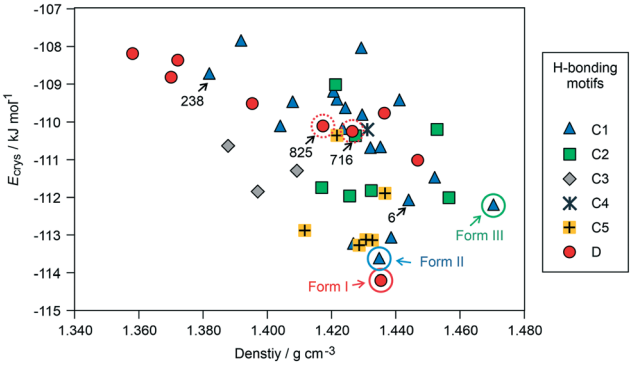

Fig. 2 Lowest-energy crystal structures for 3HBA generated in CSP searches, with the experimental structures highlighted. The structures are classified according to hydrogen-bonding motifs (defined in Fig. 3). The experimental and selected hypothetical structures are labelled/encircled.

according to strong hydrogen-bonding interactions, *i.e.* motif C or D (Fig. 3). Only one fifth of the structures in the crystal energy landscape forms the dimer motif D. Thus, the majority of the hypothetical structures features the motif C, which is in contrast to previously computed (lattice) energy landscapes of dihydroxybenzoic acids.[13,14] Fig. 2 illustrates the competition of different hydrogen-bonding possibilities between carboxylic acid and hydroxyl functions, as already seen in the two literature polymorphs. A subclassification of the motif C structures revealed that five types of interactions of the C motif, two ribbon motifs (C1 and C2) and three cross-linking options (C3–5), all based on O–H···O (acid) hydrogen bonds, are feasible. Within three kJ mol^{-1} of the global minimum structure, apart from form **I**, exclusively motif C packings are found. The C5 structures are, based on crystal energy, very competitive with the experimentally observed motifs.

A packing similarity analysis of all low-energy structures, using the program CrystalCMP (Fig. 4),[36] revealed isostructural packings for form **I**. The alternative form **I** structures (716 and 825, both $Z' = 2$), four kJ mol^{-1} less stable than the experimental arrangement, differ in the position of the phenol hydroxyl proton and thus, the directionality of the strong O(phenol)–H···O(phenol) intermolecular interactions (Fig. S7 of the ESI†). The latter might indicate disorder over two sites of the polar phenol hydrogen atom as seen in related structures (*e.g.* phloroglucinol,[37,38] gallic acid[17,39]). In case of form **II**, no isostructural packings were found in Fig. 2. The structure showing the highest resemblance with form **II**, structure 6, shares identical stacks of the C1 motif with the experimental form. In structure 6 adjacent stacks of C1 are related by translation symmetry, whereas in form **II** a glide plane is present and adjacent C1 stacks are tilted with respect to one another (Fig. S8 of the ESI†). Structure 238 is another packing arrangement that exhibits a 2-dimensional relationship with form **II**, not involving the C1 motif but adjacent C layers. The packing comparisons highlight that the motifs can, despite of the same connectivity of strong hydrogen-bonding interactions, pack in different orientations (*e.g.*, planar *vs.* tilted). The highest resemblance between different (hypothetical) structures was found between packings exhibiting the same hydrogen-bonding motifs, as expressed by lowest PS_{ab} (similarity) values in Fig. 4 and S6 of the ESI.†

From the crystal energy landscape of 3HBA (Fig. 2) it can be derived that the majority of the computed structures are packed densely, with the density values spanning the range of 1.37 to 1.47 g cm^{-3}. None of the low-energy structures features only the conformer **2**. Finally, and most important, the computational search for 3HBA forms indicates that other polymorphs might be feasible, with the C5 motif and the highest-density structure being possible targets for further experimentation.

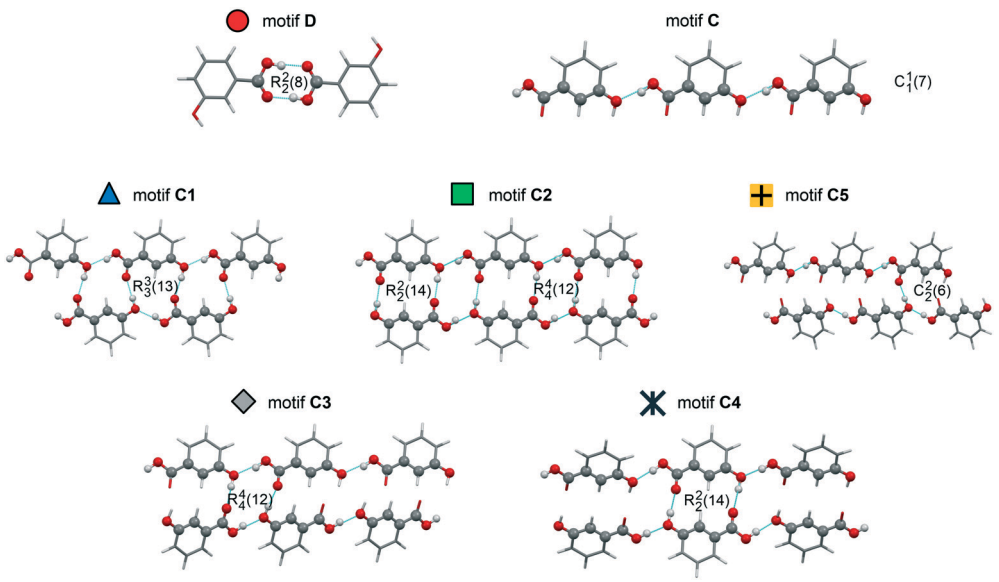

Fig. 3 Illustration of the hydrogen-bonding motifs observed in structures in the 3-hydroxybenzoic acid crystal energy landscape (Fig. 2).

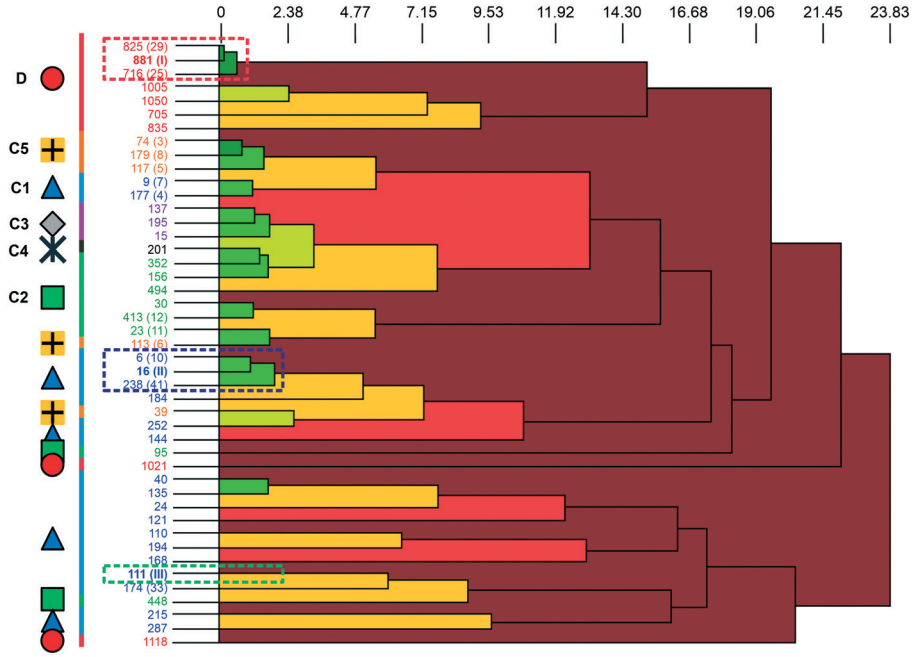

Fig. 4 The dendrogram shows the packing similarity of experimental and computed 3HBA structures. In the dendrogram the horizontal axis corresponds to the PS_{ab} value (similarity). In this case, dark green indicates almost identical packing and dark red indicates dissimilar packing. PS_{ab} values are given in the ESI.† Symbols and colour coding of the vertical axis are according to hydrogen-bonding motifs (see Fig. 3). Numbers correspond to the CrystalPredictor rank and numbers in parenthesis to either the experimental forms (I, II, III) or to the rank in Fig. 2 (given for the lowest-energy structures). For an enlarged version see Fig. S5 of the ESI.†

In the next step, the experimental forms **I** and **II** were reproduced according to literature procedures.[21] Phase identity could be confirmed using IR spectroscopy (Fig. 5) and X-ray powder diffraction (Fig. S13, ESI†). Inspired by the computed low-energy structures, preliminarily investigations related to the successful preparation of the higher density 4-aminoquinaldine Hy1B° (ref. 40) were performed, using 1-octanol instead of water. The PXRD pattern of the obtained sample featured, in addition to the reflection positions of the known polymorphs **I** and **II**, additional peaks. The experiment was then repeated without solvent in DSC heating–cooling experiments,‡ and surprisingly the crystallisation product from the melt corresponded to a distinct solid-state form (Fig. S13, ESI†).

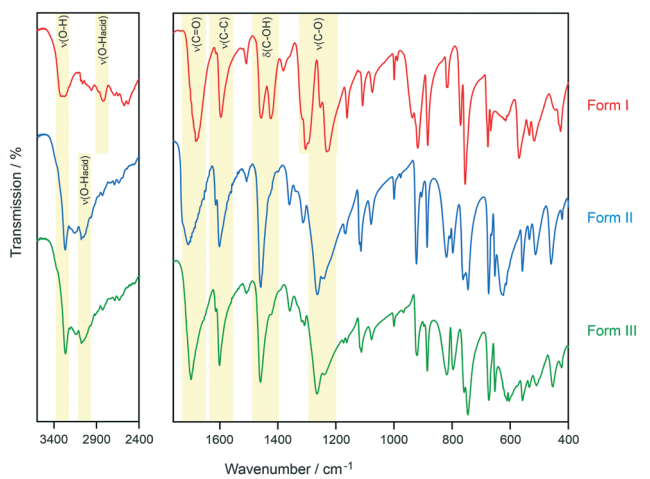

Fig. 5 Comparison of the IR spectra of the three polymorphs of 3HBA recorded at room temperature.

The IR spectrum of the polymorph obtained from the quench cooled melt (form **III** hereafter) shows high resemblance with the IR spectrum of 3HBA form **II**, with the ν(O–H) and ν(C–O) vibrational regions being nearly superimposable. The latter implies that form **III** features a C hydrogen-bonded motif (Fig. 3). A comparison of the experimental form **III** PXRD pattern to the from the computed structures simulated patterns indicates a match with the rank 9 (highest density) structure in Fig. 2. Furthermore, comparing the lattice parameters of the rank 9 structure to the experimental values (form **III** was successfully indexed[41,42] to a monoclinic $Z' = 1$ $P2_1/c$ cell) revealed a good agreement. To further confirm that the rank 9 structure corresponds to the experimental form a rigid-body Rietveld refinement[43,44] starting from a PBE-TS optimised model of the structure (see section 1.5 of the ESI†) and a structure model derived from simulated annealing[45] was carried out in tandem (Fig. S17, ESI†).§

The 3HBA molecule in the form **III** structure adopts, similar to the other two polymorphs, a conformation related to the global minimum conformer **1** (Fig. 1). As already indicated by the IR spectrum the acid forms the $C(^1_1)7$ chain motif (Fig. 3) propagating parallel to the *b* crystallographic axis. Each two $C(^1_1)7$ chains interlink through strong O–H···O (acid) hydrogen-bonding interactions forming the form **II** C1

ladder motif. The two polymorphs, form **II** and **III**, differ in the stacking of the C1 ladder and the orientation of adjacent stacks of ladders (Fig. 6). In form **II** the C1 motifs are stacked by translation symmetry along *b*, whereas in form **III** an inversion centre relates the C1 ladder motif leading to an approximate alternation of the positions of the COOH and OH functions along the *c* crystallographic axis (Fig. S20, ESI†). Adjacent stacks of ladder C1 motifs are roughly arranged in plane in **III** and tilted by approx. 133° in form **II**. Overall, the two structures exhibit only a 1-dimensional packing similarity, the C1 motif.

The stability of the experimental C1 and D motifs was estimated based on pairwise intermolecular interaction energy calculations (CrystalExplorer V17,[46–48] section 1.4 of the ESI†). The carboxylic acid dimer (form **I**) was calculated to account for −74.9 kJ mol^{-1} in pairwise energy and the additional O–H···O hydrogen-bonding interaction for twice −29.0 kJ mol^{-1}, leading to a motif D+ energy of 66.45 kJ mol^{-1}. In contrast, the C1 ladder motif was estimated to be −71.7 kJ mol^{-1} and −71.4 kJ mol^{-1} for form **II** and **III**, respectively. Thus, the ladder motif contributes more to the lattice energy than the hydrogen-bonding interactions seen in the motif D based structure **I**. Nevertheless, the slightly lower contribution from strong hydrogen-bonding interactions in form **I** is compensated for by stronger aromatic and close contact interactions, leading to a more stable packing arrangement than the C1 structures.

The thermal stability of the form **III** polymorph was investigated using hot-stage microscopy (HSM) and differential scanning calorimetry (DSC). By embedding 3HBA in high-viscosity silicon oil and then producing form **III** *via* quench cooling the melt it was possible to determine the form **III** melting point at 195.5–196.5 °C. In case of a dry preparation (without high-viscosity silicon oil) it was not possible to avoid contamination with form **I** during the procedure. In the latter experiment seed crystals of form **I** always occurred due to sublimation of the compound upon heating and induced the form **III** to **I** phase transformation (Fig. 7). Sublimation of form **I** starts at 150 °C and the transformation of form **I** to **III** at approx. 165 °C. The form **I** sublimates occur in form of stems and rectangular plates and melt at 202 °C. The HSM behaviour of 3HBA has already been described in 1954,[49] one polymorph was reported to melt at 198 °C and the other (form **I**) at 202 °C. Based on the microscopic description provided it may be concluded that the second polymorph from 1954 corresponds to form **III**.

The three polymorphs were then subjected to DSC investigations. The DSC heating curve of form **I** (Fig. 8, closed DSC pan) shows only one thermal event, the melting of the polymorph at 202 °C, with a heat of fusion ($\Delta_{fus}H$) of 36.66 kJ mol^{-1}. The latter values are in good agreement with the data determined by Nordström and Rasmuson[50] and Perlovich *et al.*[51] Upon cooling the melt, at approx. 190 °C, recrystallisation of form **III** occurs (confirmed with PXRD). Reheating form **III** in a closed DSC crucible allowed the determination of its melting point at 196 °C.

Repeating the DSC experiments with either a form **II** or a form **III** sample, with form **III** being prepared by quench cooling the melt on the hot-bench (not embedded in silicon oil), resulted at a first glance in identical DSC curves. Upon carefully examining the heating curves, exothermic phase transformations are detectable for forms **II** and **III**. In case of form **II** the transition starts at approx. 150 °C and the enthalpy value corresponds to −0.53 kJ mol^{-1} (Table 1). The transformation product is form **I**, as confirmed with variable temperature IR spectroscopy (Fig. S26, ESI†) and PXRD. The small energy difference between the two polymorphs has already been reported in literature.[50] According to the rules by Burger and Ramberger[52] it may be assumed that the polymorphic pair **II**/**I** is monotropically related, with form **I** being the stable polymorph.

Similar to form **II**, the form **III** DSC trace shows at a temperature of approx. 165 °C an exothermic transformation to form **I**, with a transition enthalpy of −1.26 kJ mol^{-1} (Table 1). The formation of form **I** was confirmed using variable temperature IR spectroscopy (Fig. S27, ESI†) and PXRD. Due to the fact that form **III** shows a lower melting point and a lower heat of fusion than form **I**, in addition to the measured exothermic transformation, it can be concluded that the polymorphic pair **III**/**I** is monotropically related. The heat of

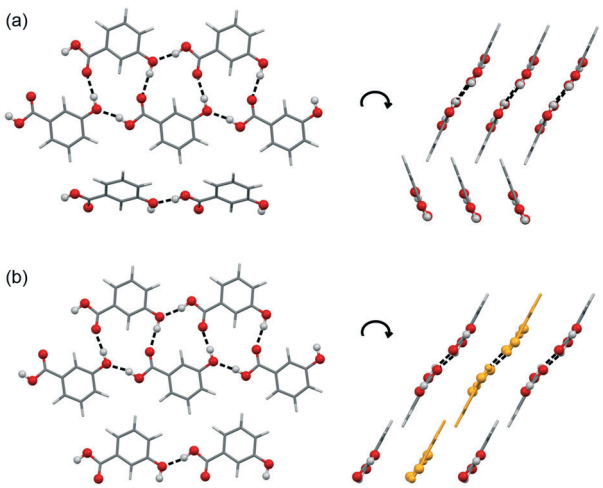

Fig. 6 Comparison of hydrogen-bonding motifs and packings of 3HBA forms **II** (a) and **III** (b). Strong H-bonding interactions are denoted with dashed lines. Ladder motifs color-coded in yellow in (b) indicate the alternative orientation of the motif (related by inversion symmetry with respect to the neighbouring ladders).

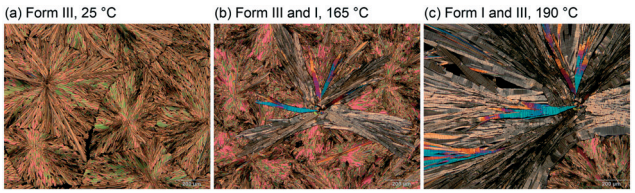

Fig. 7 Hot-stage microscopic investigations showing the 3HBA form **III** to form **I** transformation upon heating from 25 °C to 190 °C.

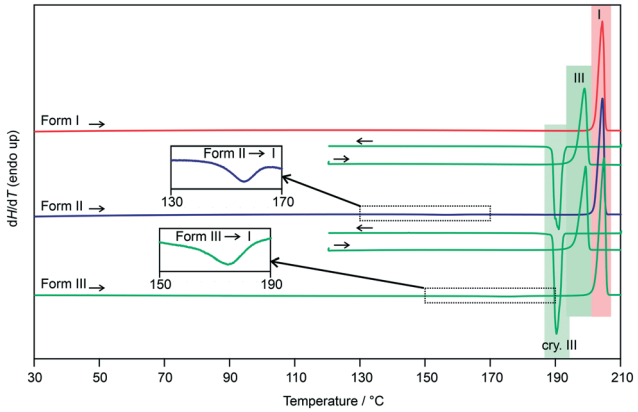

Fig. 8 DSC heating and cooling curves of 3HBA polymorphs I–III. The insets show the form II to I and form III to I phase transformations; I, III – melting points; cry – crystallisation.

fusion difference of the two polymorphs (**I** and **III**) of −2.48 kJ mol^{-1} indicates that the transition enthalpy is overestimated based on the latter calculation. The reason therefore can be seen in the fact that the compound is very volatile at high temperatures. A loss of approx. 3% of the compound was estimated if 3HBA is heated to its melting point, which was essential for preparing the form **III** sample in DSC runs.

To verify the 0 K stability order derived from DSC (Table 1), the heats of solution of the three polymorphs were recorded in DMSO (see section 2.5 of the ESI†). The heat of solution was highest for form **I** and lowest for form **III** (Table 1), resulting in an enthalpy difference of −0.64 kJ mol^{-1} and −1.03 kJ mol^{-1} for the polymorphic pairs **II/I** and **III/I**, respectively. The solution calorimetry and DSC results consistently indicate that form **I** is the most stable form, followed by form **II** and form **III** (Fig. S25 of the ESI†) and that the energy differences between the polymorphs are <1.3 kJ mol^{-1} and therefore a challenge for (lattice) energy calculations.

Based on the crystal density it can be possible to derive the 0 K stability order ('density rule'[52]). Therefore, the cell volumes of the structures determined at RT were compared. Form **III** adopts the smallest volume (611.44 Å^3) of the three polymorphs (**I**: 624.54 Å^3; **II**: 624.32–626.16 Å^3). Thus, 3HBA is an exception to the density rule, which may be due to the different hydrogen-bonding motifs seen in the experimental forms.

A comparison of the experimental and computational results shows that the method applied for the generation of the crystal energy landscape (E_{crys}, Table 1 and Fig. 2) found the experimental structures and correctly reproduced the stability order. Form **I** is calculated to be the most stable structure at all stages of the process (Table S1, ESI†). In contrast, the stability order between **II** and **III** swaps depending on whether free energy contributions are added or not. The applied method reproduced the experimental results reasonably well, but for more complex and/or more flexible molecules computationally more accurate methods should to be engaged (*e.g.*, ref. 53).

The storage stability of the metastable forms **II** and **III** was investigated at room conditions using phase pure samples and form **II** or **III** samples with form **I** impurities (1–2%). All samples were periodically analysed using PXRD. For pure form **II** and **III** samples no transition to any of the other polymorphs was observed within the investigation time of 15 weeks, whereas for the "impure" samples a very slow transformation to form **I** was already detectable after the first week (exemplarily shown in section 2.2 of the ESI† for form

Table 1 Values of the thermodynamic parameters obtained from thermal measurements, solution calorimetry and lattice energy calculations

Solid form[a]	Form **I**	Form **II**	Form **III**
Differential scanning calorimetry			
T_{fus}/°C	201.9 ± 0.1	—	195.9 ± 0.1
$\Delta_{fus}H$/kJ mol^{-1}	36.33 ± 0.18	—	33.85 ± 0.09[b]
T_{trs}/°C	—	150	165
$\Delta_{trs}H_{X-I}$/kJ mol^{-1}	—	−0.53 ± 0.02	−1.26 ± 0.13
Stability order (0 K)	*a* (most stable)	*b*	*c*
Solution calorimetry			
$\Delta_{sol}H_{(DMSO)}$/kJ mol^{-1}	−6.76 ± 0.06	−7.39 ± 0.08	−7.79 ± 0.09
$\Delta_{trs}H_{X-I}$/kJ mol^{-1}	—	−0.64 ± 0.10	−1.03 ± 0.11
Stability order (0 K)	*a* (most stable)	*b*	*c*
Calculations			
E_{latt} (DMA)/kJ mol^{-1}	−97.65	−96.87	−96.90
$-\Delta_{trs}U_{X-I}$/kJ mol^{-1}	—	−0.78	−0.75
Stability order (0 K)	*a* (most stable)	*c*	*b*
E_{latt} (CO)/kJ mol^{-1}	−100.25	−97.56	−98.48
$-\Delta_{trs}U_{X-I}$/kJ mol^{-1}	—	−2.69	−1.77
Stability order (0 K)	*a* (most stable)	*c*	*b*
E_{crys} (RT)/kJ mol^{-1}	−114.20	−113.61	−112.19
$-\Delta_{trs}U_{X-I}$/kJ mol^{-1}	—	−0.58	−2.01
Stability order (RT)	*a* (most stable)	*b*	*c*

[a] T_{fus} – melting point, $\Delta_{fus}H$ – heat of fusion, T_{trs} – transition temperature, $\Delta_{trs}H_{X-I}$ – heat of transition from form **II** or **III** to **I**, $\Delta_{sol}H_{(DMSO)}$ – heat of solution in DMSO, E_{latt} – lattice energy, DMA – DMACRYS, CO – CrystalOptimizer, E_{crys} (RT) – crystal energy estimated at 25 °C. For details see section 1.2 of the ESI.† [b] The acid is very volatile at the melting point. Therefore the $\Delta_{fus}H$ values, in particular for form **III** (produced from the melt of **I**), are too low and should not be used to calculate $\Delta_{trs}H_{III-I}$.

III spiked with form **I**). Thus, the metastable forms of 3HBA are only storage stable if phase pure. It was not possible to induce a form **III** to form **II** transformation in the solid-state.

Conclusions

3-Hydroxybenzoic acid is used as a coformer for modifying physico-chemical properties of (drug) molecules. Therefore, it is essential to have a thorough knowledge of its solid form landscape. As demonstrated in this study, understanding the solid-state, even for a small molecule, is still much a work in progress. This work highlights the potential of computational chemistry in finding and characterising solid-state forms. The fact that numerous structures in the crystal energy landscape are highly competitive in energy, despite showing different hydrogen-bonding motifs and distinct packing arrangements, explains why 3-hydroxybenzoic acid is prone for polymorphism. Based on the computational results it can be assumed that other polymorphs of the compound can exist. Furthermore, this carefully conducted study allowed to measure transition enthalpies for polymorphs which are close in energy, and thus, provides reference data for improving computational algorithms.

The author would like to thank Prof. Price (University College London) for the use of DMACRYS, Profs. Pantelides and Adjiman (Imperial College London) for the use of CrystalPredictor and CrystalOptimizer, and Prof. Griesser (University of Innsbruck) for access to instrumentation. The computational results presented have been achieved using the HPC infrastructure LEO of the University of Innsbruck.

Conflicts of interest

There are no conflicts to declare.

Notes and references

‡ 3HBA form **I** or **II** was heated in a closed DSC crucible above its melting point and then cooled to RT.

§ Crystal data of form **III**: $C_7H_6O_3$, Mr = 138.12, monoclinic, $P2_1/c$, T = 25 °C, sample formulation: powder, wavelength: 1.54184 Å, a = 9.6308(3) Å, b = 8.2989(2) Å, c = 7.7396(2) Å, β = 98.716(3), Z = 4, density = 1.500 g cm^{-3}, 2 theta range for data collection: 2 to 70°, background treatment: Chebyshev polynomial, No. of measured reflections: 265, refinement method: rigid-body (PBE-TS), data/parameter: 265/50, R_{wp} = 10.40%, R_{exp} = 1.76%, R_p = 8.17%.

1 M. von Raumer and R. Hilfiker, in *Polymorphism in the Pharmaceutical Industry*, ed. R. Hilfiker and M. von Raumer, Wiley-VCH, Weinheim, Germany, 2nd edn, 2019, pp. 1–30.
2 N. K. Duggirala, M. L. Perry, O. Almarsson and M. J. Zaworotko, *Chem. Commun.*, 2016, **52**, 640–655.
3 A. Y. Lee, D. Erdemir and M. S. Myerson, *Annu. Rev. Chem. Biomol. Eng.*, 2011, **2**, 259–280.
4 H. G. Brittain, D. J. R. Grant and P. B. Myrdal, *Drugs Pharm. Sci.*, 2009, **192**, 436–480.
5 R. Hilfiker, F. Blatter and M. von Raumer, in *Polymorphism in the Pharmaceutical Industry*, ed. R. Hilfiker, 2006, pp. 1–19.
6 Food and Drug Administration/Center for Drug Evaluation and Research (CDER), Regulatory Classification of Pharmaceutical Co-Crystals Guidance for Industry, 2018.
7 C. Zhang, Y. Xiong, F. Jiao, M. Wang and H. Li, *Cryst. Growth Des.*, 2019, **19**, 1471–1478.
8 D.-K. Bucar, R. F. Henry, G. G. Z. Zhang and L. R. MacGillivray, *Cryst. Growth Des.*, 2014, **14**, 5318–5328.
9 M. Goldyn, D. Larowska, W. Nowak and E. Bartoszak-Adamska, *CrystEngComm*, 2019, **21**, 7373–7388.
10 R. Kaur, R. Gautam, S. Cherukuvada and T. N. Guru Row, *IUCrJ*, 2015, **2**, 341–351.
11 C. Liu, C. Kuei, J. Zhu, J. Yu, L. Zhang, A. Shih, T. Mirzadegan, J. Shelton, S. Sutton, M. A. Connelly, G. Lee, N. Carruthers, J. Wu and T. W. Lovenberg, *J. Pharmacol. Exp. Ther.*, 2012, **341**, 794–801.
12 B. Sarma, P. Sanphui and A. Nangia, *Cryst. Growth Des.*, 2010, **10**, 2388–2399.
13 D. E. Braun, P. G. Karamertzanis, J.-B. Arlin, A. J. Florence, V. Kahlenberg, D. A. Tocher, U. J. Griesser and S. L. Price, *Cryst. Growth Des.*, 2011, **11**, 210–220.
14 D. E. Braun, P. G. Karamertzanis and S. L. Price, *Chem. Commun.*, 2011, **47**, 5443–5445.
15 R. A. Haak and B. W. Benson, *Int. J. Radiat. Biol. Relat. Stud. Phys., Chem. Med.*, 1973, **23**, 157–166.
16 F. L. Nordstroem and A. C. Rasmuson, *Eur. J. Pharm. Sci.*, 2006, **28**, 377–384.
17 D. E. Braun, R. M. Bhardwaj, A. J. Florence, D. A. Tocher and S. L. Price, *Cryst. Growth Des.*, 2013, **13**, 19–23.
18 G. V. Gridunova, N. G. Furmanova, Y. T. Struchkov, Z. I. Ezhkova, L. P. Grigoryeva and B. A. Chayanov, *Kristallografiya*, 1982, **27**, 267–272.
19 R. Taylor and P. A. Wood, *Chem. Rev.*, 2019, **119**, 9427–9477.
20 S. Clevers, F. Simon, M. Sanselme, V. Dupray and G. Coquerel, *Cryst. Growth Des.*, 2013, **13**, 3697–3704.
21 M. Svaerd and A. C. Rasmuson, *Cryst. Growth Des.*, 2013, **13**, 1140–1152.
22 P. G. Karamertzanis and C. C. Pantelides, *J. Comput. Chem.*, 2005, **26**, 304–324.
23 P. G. Karamertzanis and C. C. Pantelides, *Mol. Phys.*, 2007, **105**, 273–291.
24 M. Habgood, I. J. Sugden, A. V. Kazantsev, C. S. Adjiman and C. C. Pantelides, *J. Chem. Theory Comput.*, 2015, **11**, 1957–1969.
25 S. L. Price, M. Leslie, G. W. A. Welch, M. Habgood, L. S. Price, P. G. Karamertzanis and G. M. Day, *Phys. Chem. Chem. Phys.*, 2010, **12**, 8478–8490.
26 A. J. Stone, *J. Chem. Theory Comput.*, 2005, **1**, 1128–1132.
27 A. J. Stone, *GDMA: A Program for Performing Distributed Multipole Analysis of Wave Functions Calculated Using the Gaussian Program System [2.2]*, University of Cambridge, Cambridge, United Kingdom, 2010.
28 D. S. Coombes, S. L. Price, D. J. Willock and M. Leslie, *J. Phys. Chem.*, 1996, **100**, 7352–7360.
29 A. V. Kazantsev, P. G. Karamertzanis, C. S. Adjiman and C. C. Pantelides, *J. Chem. Theory Comput.*, 2011, **7**, 1998–2016.
30 A. T. Anghel, G. M. Day and S. L. Price, *CrystEngComm*, 2002, **4**, 348–355.

31 G. M. Day, S. L. Price and M. Leslie, *Cryst. Growth Des.*, 2001, **1**, 13–27.
32 G. M. Day, S. L. Price and M. Leslie, *J. Phys. Chem. B*, 2003, **107**, 10919–10933.
33 S. L. Price and S. M. Reutzel-Edens, *Drug Discovery Today*, 2016, **21**, 912–923.
34 S. L. Price, D. E. Braun and S. M. Reutzel-Edens, *Chem. Commun.*, 2016, **52**, 7065–7077.
35 M. C. Etter, *Acc. Chem. Res.*, 1990, **23**, 120–126.
36 J. Rohlicek, E. Skorepova, M. Babor and J. Cejka, *J. Appl. Crystallogr.*, 2016, **49**, 2172–2183.
37 L. H. Thomas, G. A. Craig, C. A. Morrison, A. M. Reilly and C. C. Wilson, *Cryst. Growth Des.*, 2011, **11**, 2045–2049.
38 D. E. Braun, D. A. Tocher, S. L. Price and U. J. Griesser, *J. Phys. Chem. B*, 2012, **116**, 3961–3972.
39 A. A. Hoser, I. Sovago, A. Lanza and A. O. Madsen, *Chem. Commun.*, 2017, **53**, 925–928.
40 D. E. Braun, H. Oberacher, K. Arnhard, M. Orlova and U. J. Griesser, *CrystEngComm*, 2016, **18**, 4053–4067.
41 A. J. Markvardsen, W. I. F. David, J. C. Johnson and K. Shankland, *Acta Crystallogr., Sect. A: Found. Crystallogr.*, 2001, **57**, 47–54.
42 W. I. F. David, K. Shankland, J. van de Streek, E. Pidcock, W. D. S. Motherwell and J. C. Cole, *J. Appl. Crystallogr.*, 2006, **39**, 910–915.
43 A. Coelho, *J. Appl. Crystallogr.*, 2018, **51**, 210–218.
44 H. M. Rietveld, *J. Appl. Crystallogr.*, 1969, **2**, 65–71.
45 G. S. Pawley, *J. Appl. Crystallogr.*, 1981, **14**, 357–361.
46 M. J. Turner, S. Grabowsky, D. Jayatilaka and M. A. Spackman, *J. Phys. Chem. Lett.*, 2014, **5**, 4249–4255.
47 M. J. Turner, S. P. Thomas, M. W. Shi, D. Jayatilaka and M. A. Spackman, *Chem. Commun.*, 2015, **51**, 3735–3738.
48 C. F. Mackenzie, P. R. Spackman, D. Jayatilaka and M. A. Spackman, *IUCrJ*, 2017, **4**, 575–587.
49 L. Kofler and A. Kofler, *Thermo-Mikro-Methoden zur Kennzeichnung organischer Stoffe und Stoffgemische*, Verlag Chemie GmbH, Weinheim/Bergstrasse, 1954.
50 F. L. Nordström and A. C. Rasmuson, *J. Pharm. Sci.*, 2006, **95**, 748–760.
51 G. L. Perlovich, T. V. Volkova and A. Bauer-Brandl, *J. Pharm. Sci.*, 2006, **95**, 1448–1458.
52 A. Burger and R. Ramberger, *Microchim. Acta*, 1979, **2**, 273–316.
53 J. Hoja, H.-Y. Ko, M. A. Neumann, R. Car, R. A. DiStasio and A. Tkatchenko, *Sci. Adv.*, 2019, **5**, eaau3338.